

# Basic parameters of three star clusters in the Small Magellanic Cloud: Kron 11, Kron 63 and NGC 121

G. Baume,<sup>1★†</sup> N. E. D. Noël,<sup>2★</sup> E. Costa,<sup>3★</sup> G. Carraro,<sup>4,★‡</sup> R. A. Méndez<sup>3★</sup>  
and M. H. Pedreros<sup>5★</sup>

<sup>1</sup>*Facultad de Ciencias Astronómicas y Geofísicas (UNLP), Instituto de Astrofísica de La Plata (CONICET, UNLP), Paseo del Bosque s/n, La Plata, Argentina*

<sup>2</sup>*Instituto de Astrofísica de Canarias, Tenerife 38200, Canary Islands, Spain*

<sup>3</sup>*Departamento de Astronomía, Universidad de Chile, Casilla 36-D, Santiago, Chile*

<sup>4</sup>*ESO, Alonso de Cordova 3107, Vitacura, Santiago de Chile, Chile*

<sup>5</sup>*Departamento de Física, Facultad de Ciencias, Universidad de Tarapacá, Casilla 7-D, Arica, Chile*

## ABSTRACT

We present observations for three star clusters, Kron 11, Kron 63 and NGC 121, in the Small Magellanic Cloud. We have studied their structure and derived their fundamental parameters by means of their luminosity functions, their colour magnitude diagrams and the Padova suite of isochrones. NGC 121 is a well-studied object, for which we confirm previous evidence about its old age and low-metal content, and have found that it is an undergoing mass segregation. Kron 11 and Kron 63 are poorly populated clusters which had never been studied so far. Kron 11 is several gigayears younger than NGC 121, while Kron 63 is basically a very young star aggregate. Both clusters are immersed in dense stellar fields which share the same population properties, suggesting that in their cases, cluster ages are consistent with typical ages of field stars.

**Key words:** stars: evolution – star: individual: NGC 121 – star: individual: Kron 11 – star: individual: Kron 63 – galaxies: individual: Small Magellanic Cloud – galaxies: star clusters.

## 1 INTRODUCTION

Star clusters are widely considered as single-age and single-metallicity stellar populations. This has allowed us to use them as stellar population tracers to infer the star formation history (SFH) of their parent galaxy. In particular, star clusters in the Magellanic Clouds (MC) have become a challenging domain for stellar and galactic evolutionary models because these clusters differ significantly from those found in our Galaxy. These differences are commonly attributed to the profoundly different MC environment and, hence, to a different chemical and dynamical evolution.

In this paper, we investigate three star clusters of the Small Magellanic Cloud (SMC): Kron 11 (=Lindsay 20), Kron 63 (=Lindsay 88) and NGC 121 (=Lindsay 10). We have determined their fundamental parameters: morphology, age and metallicity. The observations were secured as a part of a comprehensive study of the MC, which includes the study of stellar clusters (see e.g. NGC 2154,

Baume et al. 2007), the study of their global SFH (Noël et al. 2007, hereafter NGCM; Noël et al., in preparation) and the determination of their absolute proper motions with respect to background quasi-stellar objects (Pedreros, Costa & Méndez 2006, Costa et al., in preparation).

Kron 11 and Kron 63 had so far only been catalogued (see e.g. Kron 1956; Lindsay 1958; Bica & Schmitt 1995), and only a rough estimation of their properties was available (see Kontizas et al. 1990, and references therein). Here, we provide the first derivation of their basic properties from deep photometric observations. Adding up information on the unstudied clusters certainly may help us to better understand the age distribution of clusters in the SMC, a subject which is quite disputed (see e.g. Mighell & French 1998a; Mighell, Sarajedini & French 1998b; Rich et al. 2000; Chiosi et al. 2006; Gieles et al. 2007; Piatti et al. 2007).

NGC 121 is a very well studied cluster (see e.g. Glatt et al. 2008, and references therein). It is the oldest SMC cluster and currently considered to be the only true globular cluster in the SMC. We expected that our observations of NGC 121 would allow us to focus on conflictive aspects of previous observations of this cluster, but, unfortunately, poor photometric conditions (see Section 4) prevented us from reaching our original goal.

The layout of the paper is as follows. In Section 2, we describe the observations, and in Sections 3 and 4 we describe the reduction procedure and the photometric completeness, respectively. In

\*E-mail: gbaume@fcaglp.fcaglp.unlp.edu.ar (GB); noelia@iac.es (NN); costa@das.uchile.cl (EC); gcarraro@eso.org (GC); rmendez@das.uchile.cl (RAM); mpedreros@uta.cl (MP)

†Member of Carrera del Investigador CONICET, Argentina.

‡On leave from Dipartimento di Astronomia, Università di Padova, Vicolo Osservatorio 2, I-35122, Padova, Italy.

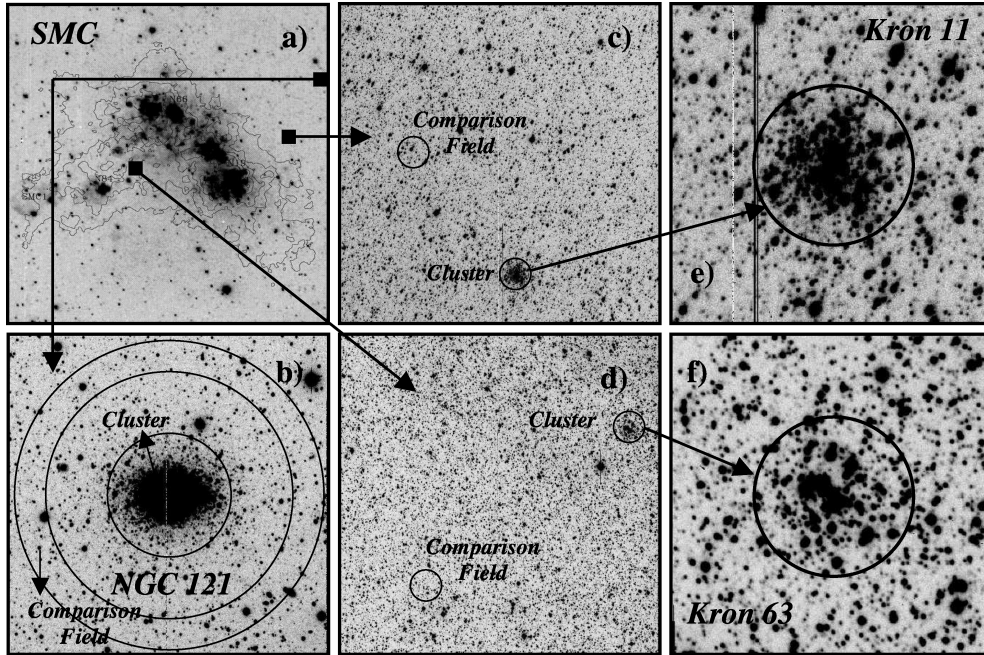


**Figure 1.** (a)  $H\alpha$  image of the SMC from Kennicutt et al. (1995) with H I contours (Stanimirović et al. 1999). Black squares indicate the approximate position of the regions observed. (b–d)  $R$ -band images of the specific fields studied in the regions of NGC 121, Kron 11 and Kron 63, respectively. The size of the regions is  $8.85 \times 8.85$  arcmin<sup>2</sup>. The circles indicate the adopted *Cluster* areas and *comparison fields* in each case (see Sections 6 and 7). (e and f) Expanded views of Kron 11 and Kron 63, respectively. In all the cases, north is up and east to the left.

Section 5, we discuss the cluster’s morphologies. In Sections 6 and 7, we present their luminosity functions (LFs) and colour–magnitude diagrams (CMDs), respectively. In Section 8, we analyse each cluster individually and, finally, in Section 9 we summarize and further discuss our results.

## 2 OBSERVATIONS AND REDUCTIONS

$B(R)_{KC}$  images of the NGC 121, Kron 11 and Kron 63 regions of the SMC were acquired with a  $24 \mu$  pixels Tektronix 2048  $\times$  2048 detector attached to the Cassegrain focus of the du Pont 2.5-m telescope (C100) at Las Campanas Observatory, Chile. Gain and read noise were  $3 e^-/ADU$  and  $7 e^-$ , respectively. This setup provides direct imaging over a field of  $8.85 \times 8.85$  with a scale of  $0.259$  pixel<sup>-1</sup>. The relatively large field of view allowed us to include the cluster and a good sample of the adjacent SMC field in each case. The  $B$  and  $R$  bandpasses were selected to satisfy the needs of both the astrometry and photometry programmes. The fields of interest are shown in Fig. 1.

Details on the observations available for NGC 121 are given in Table 1 of this paper, whereas details on the observations available for Kron 11 and Kron 63 are given in table 1 of NGCM: fields qj0036 (Kron 11) and qj0111 (Kron 63). Typical full width at half-maximum (FWHM) of the Kron 11 and Kron 63 data is about  $0.9$ , whereas a much larger value ( $\approx 1.8$ ) resulted for the NGC 121 data.

All frames were pre-processed in a standard way using the IRAF<sup>1</sup> package CCDRED. With this purpose, zero exposures and sky flats were taken every night.

<sup>1</sup> IRAF is distributed by NOAO, which is operated by AURA under cooperative agreement with the NSF.

**Table 1.** NGC 121 observations.

| Date            | Airmass | Filter | Exposure time<br>(s $\times$ $N$ ) |
|-----------------|---------|--------|------------------------------------|
| 2007 October 06 | 1.41    | $B$    | $60 \times 1$                      |
|                 | 1.45    | $B$    | $600 \times 9$                     |
| 2007 October 07 | 1.49    | $R$    | $60 \times 7$                      |
|                 | 1.52    | $R$    | $400 \times 15$                    |
|                 | 1.43    | $R$    | $600 \times 1$                     |
|                 | 1.41    | $B$    | $60 \times 7$                      |
|                 | 1.45    | $B$    | $800 \times 1$                     |

*Notes.*  $N$  indicates the number of frames obtained.

## 3 THE PHOTOMETRY

While the full reduction of the photometric data available for NGC 121 is presented here, we refer to NGCM for any details about the reduction of the Kron 11 and Kron 63 data. In fact, we limited ourselves to use that data set to derive the first estimates of the fundamental parameters of these two clusters, which happened to fall inside stellar fields observed for other purposes.

### 3.1 Standard star photometry

Our instrumental photometry was defined by the use of the Harris  $UBVRI$  filter set, which constitutes the default option at the C100 for broad-band photometry on the standard Johnson–Kron–Cousins system. On the photometric nights, standard star areas from the catalogue of Landolt (1992) were observed multiple times to determine the transformation equations relating our instrumental ( $b, r$ ) magnitudes to the standard ( $B, R_{KC}$ ) system. These standard star areas were selected to provide a wide range in colours. A few of them were followed each night up to about 2.0 airmasses to determine

**Table 2.** Transformation equations coefficients (NGC 121 observations).

|                          |                          |
|--------------------------|--------------------------|
| $b_1 = +1.058 \pm 0.025$ | $r_1 = +0.613 \pm 0.049$ |
| $b_2 = +0.213 \pm 0.019$ | $r_2 = +0.136 \pm 0.038$ |
| $b_3 = -0.043 \pm 0.004$ | $r_3 = -0.009 \pm 0.006$ |

atmospheric extinction optimally. Aperture photometry was carried out for all the standard stars using the IRAF PHOTCAL package. To tie our observations to the standard system, we used transformation equations of the form

$$b = B + b_1 + b_2 * X + b_3 (B - R)$$

$$r = R + r_1 + r_2 * X + r_3 (B - R).$$

In these equations,  $b$ ,  $r$  are the aperture magnitude already normalized to 1 s, and  $X$  is the airmass. We did not include second-order colour terms because they turned out to be negligible in comparison to their uncertainties. The values of the transformation coefficients for our NGC 121 observations are listed in Table 2, whereas those for Kron 11 and Kron 63 can be found in table 3 of NGCM.

### 3.2 Clusters and SMC field photometry

We followed the procedure outlined in Baume et al. (2007). We first averaged images taken on the same night, and with the same exposure time and filtre, to remove cosmic rays and to improve the signal-to-noise ratio of the faintest stars. Then, instrumental magnitudes and  $X$ ,  $Y$  coordinates were obtained using the point spread function (PSF) method (Stetson 1987). Finally, all data from different filters and exposures were combined and calibrated using DAOMASTER (Stetson 1992). The photometry will be made available electronically at the Centre de Données Astronomiques de Strasbourg (CDS).

In Fig. 2, we present the photometric error trends (from DAOPHOT and DAOMASTER) as a function of the  $B$  magnitude for our NGC 121 observations.

## 4 PHOTOMETRIC COMPLETENESS

In order to derive the LFs of each cluster, and to compare CMDs decontaminated of field stars with isochrones, a completeness analysis of the photometric data is required.

### 4.1 Kron 11 and Kron 63

The completeness analysis of the photometric data secured for fields  $qj0036$  and  $qj0111$  of the SMC (see NGCM) – in which Kron 11 and Kron 63 are included – was carried out by Noël et al. (in

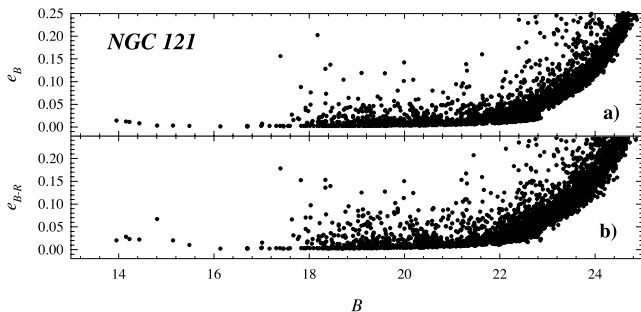


**Figure 2.** Photometric errors in  $B$  and  $B - R$ , given by DAOPHOT and DAOMASTER, plotted as a function of  $B$  magnitude (NGC 121 observations).

**Table 3.** Completeness analysis results for NGC 121.

| $\Delta$ mag | NGC 121<br>( $r < 103''.6$ ) |                             | Field                       |                             |
|--------------|------------------------------|-----------------------------|-----------------------------|-----------------------------|
|              | $B$ magnitude<br>(per cent)  | $R$ magnitude<br>(per cent) | $B$ magnitude<br>(per cent) | $R$ magnitude<br>(per cent) |
| 18.0–18.5    | 100.0                        | 100.0                       | 100.0                       | 100.0                       |
| 18.5–19.0    | 100.0                        | 99.2                        | 100.0                       | 100.0                       |
| 19.0–19.5    | 97.4                         | 87.3                        | 100.0                       | 100.0                       |
| 19.5–20.0    | 92.6                         | 78.1                        | 100.0                       | 100.0                       |
| 20.0–20.5    | 83.1                         | 64.2                        | 100.0                       | 100.0                       |
| 20.5–21.0    | 74.2                         | 61.3                        | 100.0                       | 100.0                       |
| 21.0–21.5    | 59.2                         | 57.6                        | 100.0                       | 100.0                       |
| 21.5–22.0    | 55.3                         | 46.1                        | 100.0                       | 95.2                        |
| 22.0–22.5    | 56.4                         | 32.7                        | 100.0                       | 84.4                        |
| 22.5–23.0    | 42.1                         | 30.5                        | 96.3                        | 73.2                        |
| 23.0–23.5    | 30.3                         | 23.2                        | 86.2                        | 66.7                        |
| 23.5–24.0    | 31.2                         | 21.3                        | 77.4                        | 56.5                        |
| 24.0–24.5    | 22.7                         | 15.2                        | 62.1                        | 42.7                        |
| 24.5–25.0    | 23.9                         | 13.7                        | 53.1                        | 31.9                        |
| 25.0–25.5    | 16.5                         | 10.4                        | 40.4                        | 19.6                        |
| 25.5–26.0    | 12.1                         | 7.2                         | 33.2                        | 14.4                        |
| 26.0–26.5    | 8.2                          |                             | 20.3                        |                             |

preparation), using the same technique we have applied to NGC 121. Both the photometric extraction and the completeness results are discussed there.

### 4.2 NGC 121

A completeness correction for the photometric data of NGC 121 was determined by means of artificial-star experiments (see e.g. Baume et al. 2007). We added a total of 40 000 artificial stars in random positions (with the same luminosity function as that of our real sample) to our images. To avoid the creation of overcrowding in each experiment, we added the equivalent to only 15 per cent of the original number of stars. The completeness factor is defined as the ratio between the number of artificial stars recovered and the number of artificial stars added. These ratios were computed for different  $B$  and  $R$  magnitude bins (0.5 mag wide). They are listed in Table 3, both for the cluster ( $r < 103''.6$ ) and for a representative comparison field (see Section 6.1). To obtain the completeness factor for a particular star with a given  $B - R$  colour, the corresponding factors in  $B$  and  $R$  have to be multiplied.

## 5 RADIAL DENSITY AND SURFACE BRIGHTNESS PROFILES

With the aim of deriving the clusters extension and shape, as a first step, we estimated the position of their centres searching for the highest peak in the stellar density. This was done by visual inspection of the available images. The coordinates of the cluster's centres are given in Table 4; they turned out to be very similar to those given in the SIMBAD data base.

We then compute the cluster's size, which was done constructing radial profiles using two methods (see Baume et al. 2007): the radial stellar density profile and the radial surface brightness profile. In the first method, stars are counted in a number of successive concentric rings around the adopted cluster centre, and then a division is made by the respective areas. In the second method, the flux ( $ADUs/area$ ) within concentric annuli is measured directly on the cluster images.

**Table 4.** Main properties of the studied star clusters.

| Object  | $X$<br>$Y$ | $\alpha_{2000}$<br>$\delta_{2000}$ | Radius     | $V_O - M_V$<br>$E(B - V)$ | $z$<br>$\log[\text{age}(\text{yr})]$ |
|---------|------------|------------------------------------|------------|---------------------------|--------------------------------------|
| Kron 11 | 1166       | 00:36:23.6                         | 25'0–30'0  | 18.7                      | 0.0010                               |
|         | 1285       | −72:28:39.0                        |            | 0.05                      | 9.70–9.80                            |
| Kron 63 | 1850       | 01:10:47.3                         | 20'0–25'0  | 18.7                      | 0.0006                               |
|         | 615        | −72:47:34.4                        |            | 0.07                      | 7.75–8.00                            |
| NGC 121 | 1030       | 00:26:48.2                         | 70'0–200'0 | 19.1                      | 0.0006                               |
|         | 1025       | −71:32:07.3                        |            | 0.04                      | 10.0–10.1                            |

A measure of the cluster’s radius was obtained by fitting an EEf model (see Elson, Fall & Freeman 1987), appropriate for MC clusters (Mackey & Gilmore 2003). The expression used was

$$\mu = \mu_0 [1 + (r/a)^2]^{-\gamma/2} + \phi,$$

where  $r$  is the distance from the adopted cluster centre,  $\mu_0$  is the central surface brightness,  $a$  is a measure of the core radius,  $\gamma$  is the power-law slope at large radii and, finally,  $\phi$  is the field surface brightness. The resulting profiles together with the computed parameters are presented in Figs 3 and 4.

## 6 OBSERVED LUMINOSITY FUNCTIONS

To obtain the observed LFs of the clusters, we first counted the stars in each apparent magnitude bin, both in the *cluster* area and in their respective *comparison field* (see Fig. 1). In each case, they were corrected by the completeness factors given in Section 4. The resulting histograms are shown in the upper panels of Fig. 5. A cleaner picture of the cluster’s population is obtained by subtracting these histograms in the sense *cluster*–*field*. The results are shown in the lower panels of Fig. 5.

## 7 COLOUR–MAGNITUDE DIAGRAMS

In Fig. 6, we present CMDs for Kron 11 and Kron 63, and in Fig. 7 we present CMDs for NGC 121. Left-hand panels show CMDs for stars measured in the selected areas indicated as *cluster*, while the central panels show CMDs for stars measured in the selected areas indicated as *comparison field* in Fig. 1. These latter were chosen at appropriate distances from the cluster centres to minimize the presence of cluster stars in them. These figures show that the *cluster* CMDs suffer an important contamination by the SMC field stars.

To obtain better estimates of clusters characteristics, we applied the statistical decontamination method of the CMDs described in Vallenari et al. (1992) and Gallart et al. (2003), and used in our study of NGC 2154 (Baume et al. 2007). In this procedure, a statistical subtraction of field stars is carried out by making a star-by-star comparison between the selected *comparison field* and the *cluster* area. Briefly, for any given star in the *comparison field* we search for the most similar (in colour and magnitude) star in the *cluster* area, and remove it from the corresponding CMD. It should be noted that this procedure takes into account the difference in completeness level between the *cluster* area and their *comparison field*, and also the increase in the photometric error with increasing magnitude (the search ellipse is a function of the magnitude to take into account this latter effect). Figs 6(c), 6(f) and 7(c) present the resulting decontaminated CMDs.

Quick inspection of Figs 6 and 7 shows that our observations of NGC 121 are clearly less deep than those of Kron 11 and Kron 63.

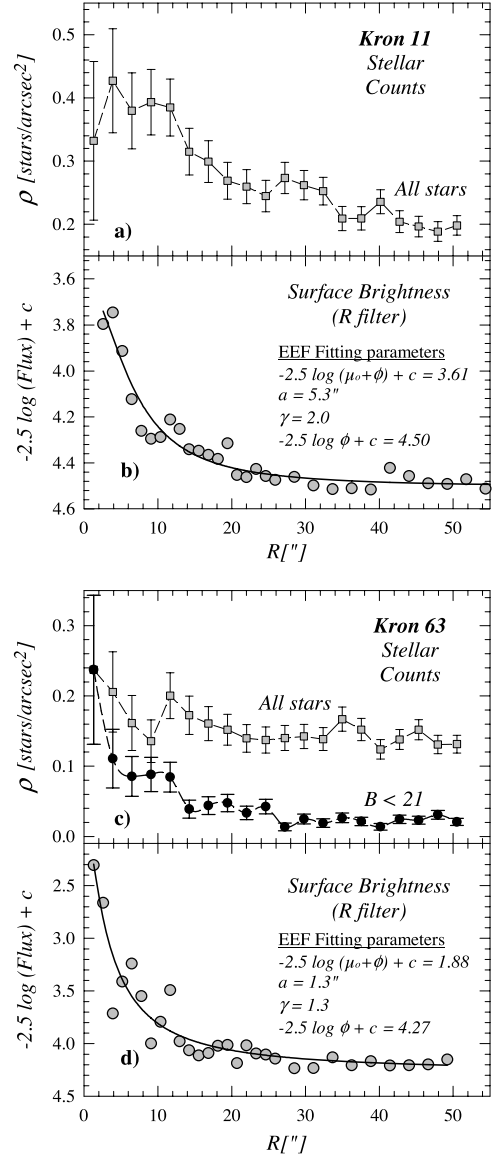


**Figure 3.** Radial profiles for Kron 11 and Kron 63. (a) and (c) Radial stellar density profiles. (b) and (d) Radial flux profiles (grey circles) and the EEf model fits (solid curves) together with the computed fitted parameters.  $c$  is an arbitrary constant with a different value for each cluster.

Comparison of the data presented in Table 1 of this work with that presented in Table 1 of NGCM shows that although total exposure time is a factor, the main reason for this difference is the worse seeing conditions throughout our NGC 121 observing runs ( $\approx 1''.8$ ), amplified by crowding in the much denser NGC 121 field.

Interestingly, the three clusters share the same stellar population features of the SMC field they are immersed in. NGC 121 and Kron 11 are located in old fields, and look old, whereas Kron 63 is located in a younger field, and appears to be young. It should be noted that these stellar populations are typical of the north-west and south-east regions of the SMC (see NGCM for details).

To derive the cluster’s basic parameters (age and metallicity), we compared their CMDs with theoretical isochrones from the Padova stellar evolution models (Girardi et al. 2000). The selection of the metallicities was done choosing those isochrones that produce the best fit to the red giant branch (RGB) – when present – and to

## 8 INDIVIDUAL CLUSTER ANALYSIS

### 8.1 Kron 11

The radial profiles of this object (Figs 3a and b) reveal the clear presence of a cluster above the stellar field up to a distance of about 25–30 arcsec from the adopted centre. The surface brightness profile presents, however, a moderate spread around the fitted curve of the EEf radial model. This fact is due the poor radial symmetry of the object (see Fig. 1e).

As previously noted, the CMDs of this cluster and its *comparison field* (Figs 6a and b), do not show significant differences between them, in the sense that they are apparently composed by similar stellar populations. However, according to its corrected LF (see Fig. 5b), the cluster produces a clear overdensity of stars corresponding to its MS and a horizontal branch (HB). Test fits with several isochrones of different age and metallicity indicate that this cluster has a slightly higher metallicity than that normally adopted for the SMC (Maeder, Grebel & Mermilliod 1999).

With an age of  $\sim 6$  Gyr, Kron 11 sums up to the intermediate-age group of SMC star clusters which fall in the LMC age gap (Girardi et al. 1995). Although the percentage of star clusters in this age range is still poorly constrained (Rafelski & Zaritsky 2005), the present result points out to a clear difference in the rate of cluster formation in between the MCs.

### 8.2 Kron 63

This cluster appears as a weak concentration of bright stars against the rich SMC field. Before analysing the properties of this overdensity, we can test its reality by means of a *t*-Student test. A comparison of its corrected LF (see Fig. 5d) with typical stellar fluctuations present in the rest of the observed region shows that the Kron 63 ‘fluctuation’ is four times larger than the average stellar field fluctuations. Applying these values to a *t*-Student test, we obtain a nearly 100 per cent of reliability, meaning that Kron 63 is a real star cluster, and not just a statistical fluctuation of the field population.

Examination of the radial profile of this object (Fig. 3c) shows that if all detected stars are taken into account it does not stand out clearly over the field, but, if only the brightest stars are considered ( $B < 21$ ), the cluster becomes more prominent and we find that it is composed mainly of blue stars ( $B - R < 0.5$ ). The surface

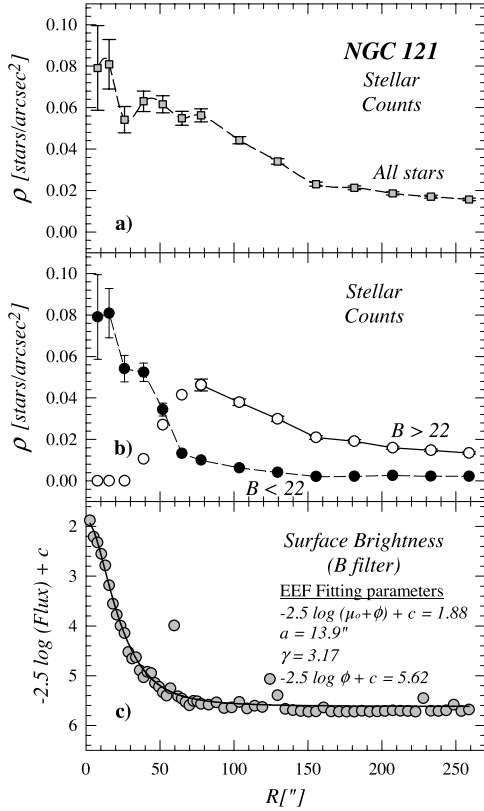


**Figure 4.** Radial profiles for NGC 121. (a) Radial stellar density profiles. (b) Radial stellar density profiles for two different magnitude intervals. (c) Radial flux profile (grey circles) and the EEf model fit (solid curve) together with the computed fitted parameters.  $c$  is an arbitrary constant.

the main sequence (MS). To perform the above comparisons, it was necessary to adopt a distance modulus and to assume a mean value for the reddening of each cluster. These values are indicated in Table 4 and they are consistent with several previous estimates (see next sections). In all the cases, the normal relations:  $E(B - R) = 1.57 E(B - V)$  and  $B - M_B = (V_O - M_V) + 4.1 E(B - V)$ , have been adopted to calculate the colour excess and the apparent distance modulus, respectively.

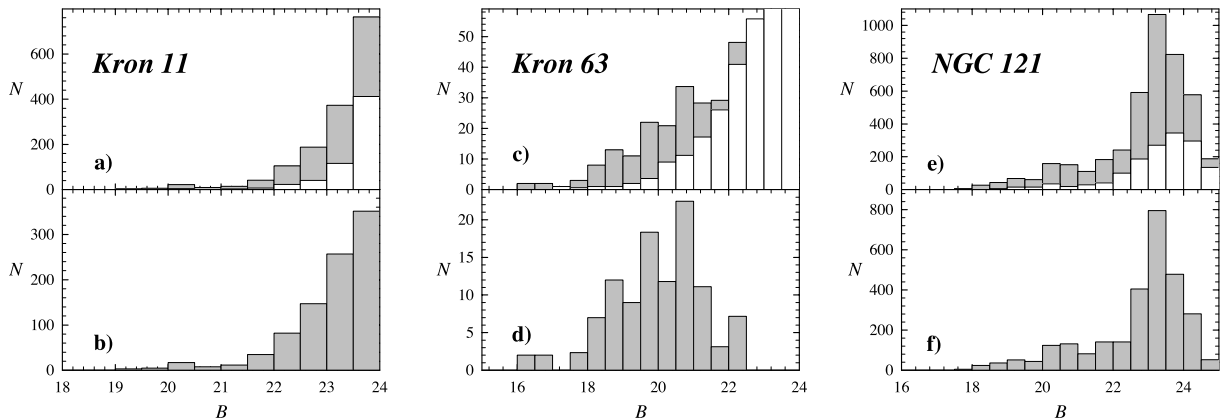


**Figure 5.** (a), (c) and (e) Luminosity functions corrected by completeness factors (see Section 4). Grey histogram corresponds to the *cluster* areas, whereas the white histogram corresponds to the respective *comparison field* areas. (b), (d) and (f) Luminosity functions obtained for each cluster after the correction by field contamination.

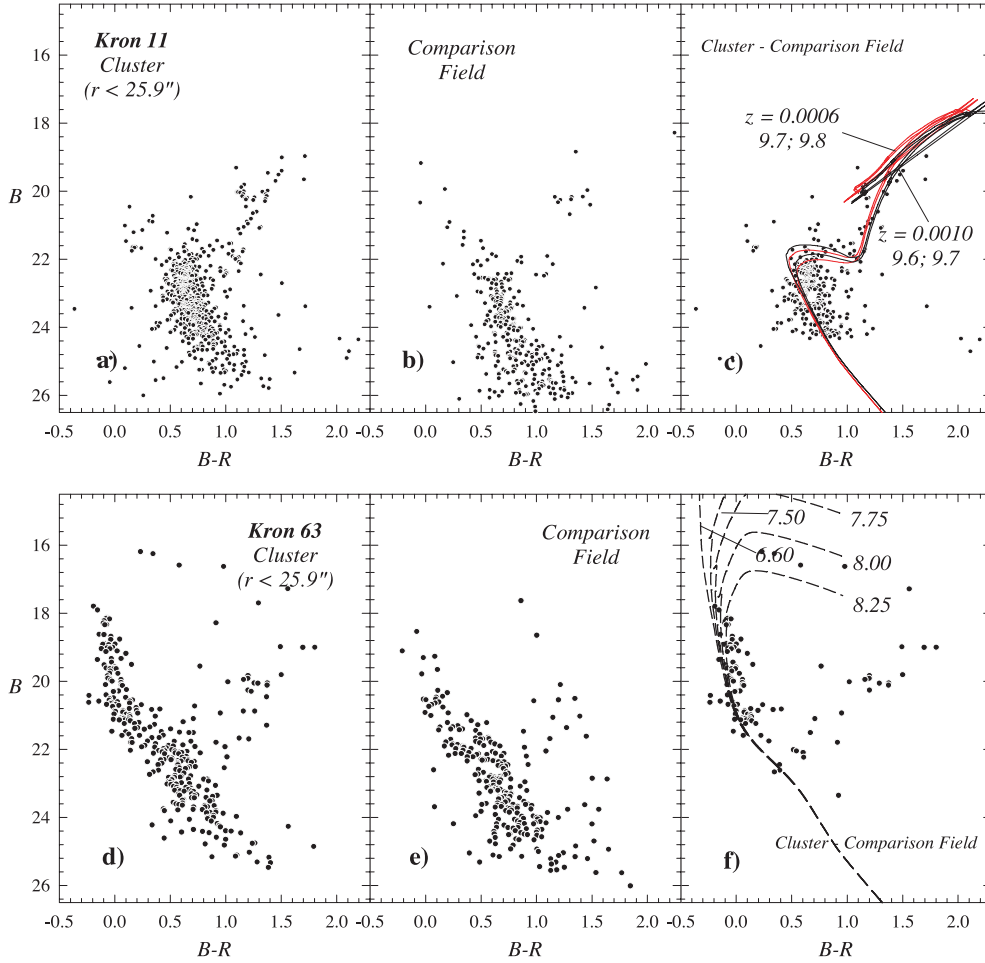


**Figure 6.** CMDs of Kron 11 and Kron 63. Left-hand panels (a and d) are the CMDs of stars placed in the *cluster* areas. Central panels (b and e) are the CMDs of stars in the respective comparison field. Right-hand panels (c and f) present the statistical difference between the other panels (cluster area – comparison field). The solid curves are the best-fitting isochrones from Girardi et al. (2000). Numbers indicate  $\log[\text{age}(\text{yr})]$  and adopted metallicities.

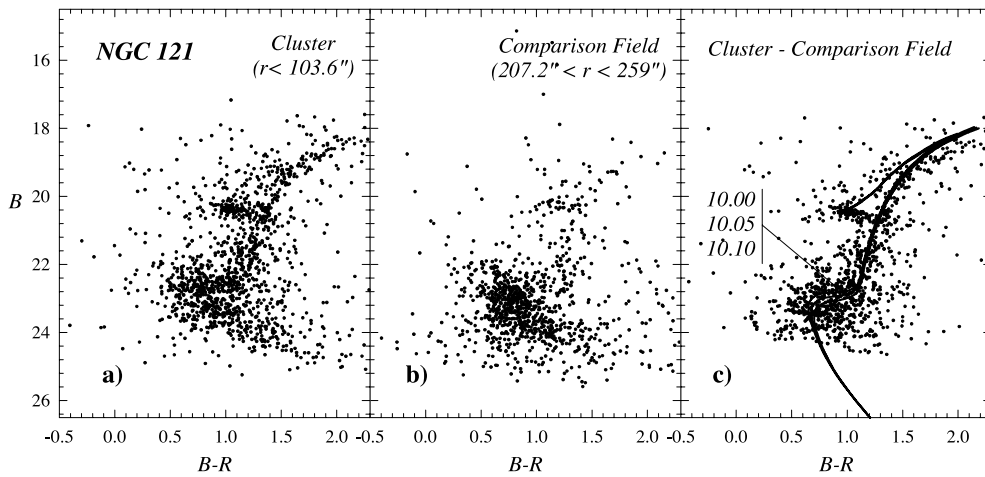


**Figure 7.** CMDs of NGC 121 observations. Panels have the same meaning as in Fig. 6.

brightness profile of this object also presents an important spread around the fitted curve of the EEF radial model (see Fig. 3d). Both radial profiles indicate, however, that this cluster extends up to a distance of about 20–25 arcsec from the adopted centre.

The CMDs of this cluster (Figs 6c and d) exhibit characteristics typical of an object much younger than Kron 11; it presents a significant MS population in an ample range of magnitudes and it does not seem to possess luminous red stars. Therefore, the best

isochrone was found on the basis of the MS morphology, and adopting a metallicity considered normal for the SMC (see Table 4).

We note that after the decontamination process the MS of Kron 63 shortens significantly compared to that of Kron 11. This can be explained by the difference in mass between the two clusters. As shown by the radial density profiles derived in Section 5 (and by Fig. 1), although significantly older, Kron 11 still looks more compact and massive than Kron 63. At birth, Kron 11 must have been more massive than Kron 63, and, having a larger potential well, it has survived longer and managed to retain a larger number of low-mass stars. Low-mass star-depleted MSs are not rare, and often found, at different ages, in Milky Way star clusters (Patat & Carraro 1995; Bica et al. 2001; Nordstrom, Andersen & Andersen 1997).

### 8.3 NGC 121

The radial profile based on stellar counts (Fig. 4a), clearly shows the limitations of the data available for this cluster due to poor seeing conditions, as mentioned in Section 5. This is reflected in the very low stellar density values obtained for this object. It is still possible, however, to describe some cluster properties by selecting appropriate magnitude intervals (Fig. 4b), and by means of the surface brightness profile (Fig. 4c). Both plots reveal the following issues.

(i) The adopted EEF profile fits nicely to the data, indicating that this cluster is very well represented by this model.

(ii) The total cluster brightness is dominated by the brightest stars and the cluster is apparently extending up to near 70 arcsec of the adopted centre.

(iii) If only the faintest stars are included ( $B > 22$ ), then the radial extension can reach up to 200 arcsec from that centre. This difference in radius can be interpreted as a product of the relaxation process suffered by the cluster, causing that the massive (brightest) stars move to its centre and low-mass (faintest) stars to its outskirts.

Due to peculiarities in the distribution of field stars across the cluster region, a very efficient decontamination of the CMD of NGC 121 was not possible. Inspection of Fig. 7c shows that in the clean CMD, there are several groups of stars that are more numerous than in the field, despite the fact that both regions have the same area. In the clean CMD, some field stars still remain above the MS, to the left-hand side of the MS and everywhere in the red clump region. This effect surely results from the statistically low number of stars in those regions of the CMD. None the less, the procedure was very effective and helped us to improve the shape of the turn-off region (TO), and to remove several field RGB and HB stars.

Because there are good (and deeper) previous studies of this object (see e.g. Glatt et al. 2008, and references therein) here, we limit ourselves to check that their derived parameters are compatible with our photometry. We achieved the best fit using the parameters given in Table 4. As found by Glatt et al. (2008), we highlight the notable difference between theoretical models and observations in the upper RGB region. Model predictions are systematically bluer and more luminous than the observed RGBs, irrespective of the adopted passband.

## 9 CONCLUSIONS

We present and discuss deep  $BR$  photometry of three star clusters in the SMC: Kron 11, Kron 63 and NGC 121. We have derived

radial density, surface brightness profiles and LFs for these clusters. NGC 121 is a well-known compact cluster, but Kron 11 and Kron 63 are notably less prominent. We confirm that Kron 63 (the less conspicuous of these latter two) is a real object, which resembles more a Galactic than a globular cluster. These basic conclusions are confirmed by the  $\gamma$  value of their profile fit, from a shallow exponent of 1.3 for Kron 63 giving it a looser appearance in the sky, to the sharper NGC 121 cluster with a  $\gamma$  value of 3.17.

From the analysis of deep LFs and CMDs, we provide for the first time estimates of the main parameters of Kron 11 and Kron 63. While Kron 11 is an intermediate-age cluster, Kron 63 is significantly younger. Interestingly, both clusters look coeval to the surrounding stellar field.

We have confirmed the metallicity and age values previously estimated for NGC 121; and found a clear mass segregation effect, a process that is expected to happen in a cluster as old as it is.

## ACKNOWLEDGMENTS

GB acknowledges support from the Chilean *Centro de Astrofísica* FONDAF No. 15010003 and CONICET (PIP 5970). EC and RAM acknowledge support by the Fondo Nacional de Investigación Científica y Tecnológica (proyecto No. 1050718, Fondecyt) and the Chilean *Centro de Astrofísica* FONDAF No. 15010003. CG and NN acknowledge support by the Instituto de Astrofísica de Canarias (P3-94) and the Ministry of Education and Research of the Kingdom of Spain (AYA2004-06343).

## REFERENCES

- Baume G., Carraro G., Costa E., Méndez R. A., Girardi L., 2007, *MNRAS*, 375, 1077
- Bica E. L. D., Schmitt H. R., 1995, *ApJS*, 101, 41
- Bica E., Santiago B. X., Dutra C. M., Dottori H., de Oliveira M. R., Pavani D., 2001, *A&A*, 366, 827
- Chiosi E., Vallenari A., Held E. V., Rizzi L., Moretti A., 2006, *A&A*, 452, 179
- Elson R. A. W., Fall S. M., Freeman K. C., 1987, *ApJ*, 323, 54
- Gallart C., Freedman W. L., Aparicio A., Bertelli G., Chiosi C., 1999, *AJ*, 118, 2245
- Gallart C. et al., 2003, *AJ*, 125, 742
- Gieles M., Lamers H. J. G. L. M., Portegies Z., Simon F., 2007, *ApJ*, 668, 268
- Girardi L., Chiosi C., Bertelli G., Bressan A., 1995, *A&A*, 298, 87
- Girardi L., Bressan A., Bertelli G., Chiosi C., 2000, *A&AS*, 141, 371
- Glatt K. et al., 2008, *AJ*, 135, 1106
- Kennicutt R. C. Jr, Bresolin F., Bomans D. J., Bothun G. D., Thompson I. B., 1995, *AJ*, 109, 594
- Kontizas E., Kontizas M., Sedmak G., Smareglia R., Dapergolas A., 1990, *AJ*, 100, 425
- Kron G. E., 1956, *PASP*, 68, 125
- Landolt A. U., 1992, *AJ*, 104, 340
- Lindsay E. M., 1958, *MNRAS*, 118, 172
- Mackey A. D., Gilmore G. F., 2003, *MNRAS*, 338, 120
- Maeder A., Grebel E. K., Mermilliod J.-C., 1999, *A&A*, 346, 459
- Mighell K. J. S. A., French R. S., 1998a, *AJ*, 116, 2395
- Mighell K. J., Sarajedini A., French R. S., 1998b, *ApJ*, 494, L189
- Noël N. E. D., Gallart C., Costa E., Méndez R. A., 2007, *AJ*, 133, 2037 (NGCM)
- Nordstrom B., Andersen J., Andersen M. I., 1997, *A&A*, 322, 460
- Patat F., Carraro G., 1995, *A&AS*, 114, 281
- Pedros M. H., Costa E., Méndez R. A., 2006, *AJ*, 131, 1461

Piatti A. E., Sarajedini A., Geisler D., Gallart C., Wischnjewsky M., 2007, MNRAS, L381  
Rafelski M., Zaritsky D., 2005, AJ, 129, 2701  
Rich R. M., Shara M., Fall S. M., Zurek D., 2000, AJ, 119, 197  
Stanimirovic S., Staveley-Smith L., Dickey J. M., Sault R. J., Snowden S. L., 1999, MNRAS, 302, 417  
Stetson P. B., 1987, PASP, 99, 191

Stetson P. B., 1992, in Bulter C. J., Elliot I., eds, Proc. IAU Coll. Symp. 136, Stellar Photometry-Current Techniques and Future Developments. Cambridge Univ. Press, Cambridge, p. 291  
Vallenari A., Chiosi C., Bertelli G., Meylan G., Ortolani S., 1992, AJ, 104, 1100

This paper has been typeset from a  $\text{\TeX/L\AA\TeX}$  file prepared by the author.